J Geod (2014) 88:273–282
DOI 10.1007/s00190-013-0684-6

ORIGINAL ARTICLE

# Improved one/multi-parameter models that consider seasonal and geographic variations for estimating weighted mean temperature in ground-based GPS meteorology

**Yibin Yao · Bao Zhang · Chaoqian Xu · Feng Yan**

Received: 8 July 2013 / Accepted: 23 November 2013 / Published online: 5 December 2013


**Abstract** In ground-based GPS meteorology, weighted mean temperature is the key parameter to calculate the conversion factor which will be used to map zenith wet delay to precipitable water vapor. In practical applications, we can hardly obtain the vertical profiles of meteorological parameters over the site, thus cannot use the integration method to calculate weighted mean temperature. In order to exactly calculate weighted mean temperature from a few meteorological parameters, this paper studied the relation between weighted mean temperature and surface temperature, surface water vapor pressure and surface pressure, and determined the relationship between, on the one hand, the weighted mean temperature, and, on the other hand, the surface temperature and surface water vapor pressure. Considering the seasonal and geographic variations in the relationship, we employed the trigonometry functions with an annual cycle and a semi-annual cycle to fit the residuals (seasonal and geographic variations are reflected in the residuals). Through the above work, we finally established the GTm-I model and the PTm-I model with a $2^\circ \times 2.5^\circ$(lat × lon) resolution. Test results show that the two models both show a consistent high accuracy around the globe, which is about 1.0 K superior to the widely used Bevis weighted mean temperature–surface temperature relationship in terms of root mean square error.

**Keywords** GPS meteorology · Weighted mean temperature · Zenith wet delay · Precipitable water vapor

**Abbreviations**

| | |
|---|---|
| COSMIC | Constellation observing system of meteorology, ionosphere, and climate |
| ECMWF | European Centre for Medium-Range Weather Forecasts |
| GPS | Global Positioning System |
| IGRA | Integrated global radiosonde archive |
| IGS | International GNSS service |
| NWP | Numerical weather prediction |
| PWV | Precipitable water vapor |
| RMSE | Root mean square error |
| ZHD | Zenith hydrostatic delay |
| ZTD | Zenith total delay |
| ZWD | Zenith wet delay |

## 1 Introduction

Water vapor, an important component of the atmosphere, is mainly distributed in the lower atmosphere, and water vapor in the troposphere constitutes approximately 99 % of its total content. Although water vapor is only a minor constituent of the atmosphere in terms of its mass, it plays key roles in both the weather and climate systems (Rocken et al. 1993). The advection of water vapor and its latent heat by the general circulation of the atmosphere is an important component of

**Electronic supplementary material** The online version of this article (doi:10.1007/s00190-013-0684-6) contains supplementary material, which is available to authorized users.

Y. Yao (✉) · B. Zhang · C. Xu · F. Yan
School of Geodesy and Geomatics,
Wuhan University, Wuhan 430079, China
e-mail: ybyao@whu.edu.cn

B. Zhang
e-mail: whusggzb@gmail.com

C. Xu
e-mail: cqxu@whu.edu.cn

F. Yan
e-mail: 642304401@qq.com

the Earth's meridional energy balance (Bevis et al. 1992). A good understanding of the distribution of water vapor is necessary for weather forecasting and climate prediction (Jacob 2001).

When electromagnetic signals sent by satellites in Global Positioning System (GPS) propagate through the neutral atmosphere, they undergo two effects, i.e. time delay and bending, resulting in signal propagation delay. In GPS, this delay is called tropospheric delay. The tropospheric delay can be modeled in two parts: the delay experienced in the zenith direction and the scaling of that delay to the delay experienced at the zenith angle of the raypath under the assumption that the neutral atmosphere is both vertically stratified and azimuthally symmetric. The zenith total delay (ZTD) consists of two parts: delay caused by the atmospheric gases in hydrostatic equilibrium which is called Zenith Hydrostatic Delay (ZHD) and delay caused by those gases (primarily water vapor) not in hydrostatic equilibrium which is called Zenith Wet Delay (ZWD). Precipitable water vapor (PWV) refers to the height of the column of liquid water that would result if it were possible to condense all the water vapor in the overlying column of the atmosphere (Yao et al. 2012). Askne and Nordius (1987) derived the approximate relationship between ZWD and PWV, making it possible to use the GPS to detect water vapor. Bevis et al. (1992) first proposed the concept of GPS meteorology, introduced the principle of using GPS to detect water vapor in detail, and proposed a method to calculate weighted mean temperature ($T_\mathrm{m}$), the key parameter to map ZWD to PWV, making GPS an important mean to detect water vapor. Ding (2009) elaborated on the principles of the GPS meteorology and the related calculation method. The relationship between PWV and ZWD can be expressed as (Bevis et al. 1994):

$$\mathrm{PWV} = \Pi \cdot \mathrm{ZWD} \tag{1}$$

where $\Pi$ is water vapor conversion factor, which can be expressed as

$$\Pi = \frac{10^6}{\rho_\mathrm{w} R_\mathrm{v} \left[(k_3/T_\mathrm{m}) + k_2'\right]} \tag{2}$$

where $\rho_\mathrm{w}$ is the density of water, $R_\mathrm{v}$ is the specific gas constant for water vapor, $k_2'$, $k_3$ are the atmospheric refractivity constants (Davis et al. 1985; Bevis et al. 1994), $T_\mathrm{m}$ is the key variable to calculate the conversion factor $\Pi$ and is related to temperature and vapor pressure, and can be precisely calculated by:

$$\mathrm{T_m} = \frac{\int_{h_\mathrm{s}}^{\infty} \frac{e}{T}\,\mathrm{d}h}{\int_{h_\mathrm{s}}^{\infty} \frac{e}{T^2}\,\mathrm{d}h} \tag{3}$$

where $e$ and $T$ are the water vapor pressure (hPa) and temperature (Kelvin) of the atmosphere respectively and $h$ is the elevation (meter), $h_\mathrm{s}$ is the station height, the integral is with respect to the vertical dimension, from the surface to the top of the atmosphere. When we map ZWD to PWV, one of the largest error sources is the calculation of $\Pi$, whose relative error basically equals to that of $T_\mathrm{m}$ (Bevis et al. 1994), so exactly determining $T_\mathrm{m}$ is very important to precise calculation of PWV.

Besides the error source of $T_\mathrm{m}$, the estimate of PWV is also affected by other error sources. We could find the error sources of PWV by taking the derivative with respect to $T_\mathrm{m}$ and ZWD according to Eqs. (1) and (2). The following equations could express how the errors from $T_\mathrm{m}$ and ZWD affect PWV.

$$\sigma_\mathrm{PWV} = \mathrm{ZWD}^* \sigma_\Pi + \Pi^* \sigma_\mathrm{ZWD} \tag{4}$$

$$\sigma_\Pi = \frac{10^6 k_3}{\rho_\mathrm{w} R_\mathrm{v} (k_3 + k_2' T_\mathrm{m})^2} \sigma_{T_\mathrm{m}} \tag{5}$$

where $\sigma_\mathrm{PWV}$, $\sigma_\Pi$, $\sigma_\mathrm{ZWD}$, $\sigma_{T_\mathrm{m}}$ are error from PWV, $\Pi$, ZWD and $T_\mathrm{m}$. If we take an average of $T_\mathrm{m}$ and $\Pi$, the average $T_\mathrm{m}$ is approximate 281 K and the $\Pi$ is approximate 0.15 (ZWD in mm). Then, the Eqs. (4) and (5) can be simplified to:

$$\sigma_\mathrm{PWV} = 5.6060 \times 10^{-4} \mathrm{ZWD}^* \sigma_{T_\mathrm{m}} + 0.15^* \sigma_\mathrm{ZWD} \tag{6}$$

$$\sigma_\Pi = 5.6060 \times 10^{-4} \sigma_{T_\mathrm{m}} \tag{7}$$

If ZWD at some site in the tropics is 400 m, the estimate error of PWV caused by $T_\mathrm{m}$ is approximate 0.9 mm with BTm model. However, the error of ZWD comprises both geodetic error associated with the ZTD estimate and the error associated with predicting ZHD using a barometer, or using a climatological model, or using a numerical weather model, so the precision of ZWD estimation varies much. With a barometer, the ZWD can be recovered from GPS and VLBI data with an accuracy between 5 and 20 mm (Bevis et al. 1992). In fact, the new ZTD product provided by the International GNSS Service (IGS) is shown to possess typical formal errors of 1.5–5 mm (Byun and Bar-Sever 2009), as the ZHD can be modeled with an accuracy of a few millimeters or better given surface pressure measurements (Bevis et al. 1992), the ZWD could also achieve a better accuracy. If the ZWD error is 1 cm, the error of PWV estimate caused by ZWD error is only 1.5 mm, so we need to consider improving the accuracy of $T_\mathrm{m}$ estimate under this circumstance.

A common approach is to estimate $T_\mathrm{m}$ from the observed surface temperature ($T_\mathrm{s}$) and predetermined linear regression coefficients instead of Eq. (3). Bevis et al. 1992 found that $T_\mathrm{m}$ and $T_\mathrm{s}$ have a good linear correlation based on an analysis of 8,718 radiosonde profiles at latitudes N27°−N65° in North America, and suggested that $T_\mathrm{m}$ is linearly related to $T_\mathrm{s}$, i.e., $T_\mathrm{m} = a + bT_\mathrm{s}$. He also specified this linear relationship to $T_\mathrm{m} = 70.2 + 0.72T_\mathrm{s}$. Later in 1995, Bevis et al. modified this equation to $T_\mathrm{m} = 85.63 + 0.668T_\mathrm{s}$ based on $\sim$ 250, 000 radiosonde profiles which were evenly distributed around the globe. However, the relationship between $T_\mathrm{m}$

and $T_s$ changes with locations and seasons, for best results, the coefficients $a$ and $b$ should be calculated for specific areas and seasons (Bevis et al. 1992; Ross and Rosenfeld 1997). Li et al. (1999) established the monthly $T_m-T_s$ relationship suitable for use in eastern China. Wang et al. (2007) established similar linear relation for use in Wuhan region. Wang et al. (2011) concluded that there is no significant difference between one-factor ($T_s$) and multi-factor ($T_s$, surface pressure $P_s$, surface water vapor pressure $e_s$) linear regression results, but the accuracy of regression relation based on local radiosonde data is higher than that of Bevis $T_m-T_s$ relationship for local use. Yao et al. (2012) took seasonal and geographic variations into account, established the empirical model GWMT based on spherical harmonics, well solving the problem of calculating $T_m$ independent of measured meteorological parameters.

However, the short time period and limited domain involved in the above linear regression models (Bevis et al. 1992; Li et al. 1999; Wang et al. 2007, 2011) precluded the examination of the seasonal or geographic variability. Thus, there is uncertainty regarding the accuracy and appropriateness of those coefficients for general use. Though the GWMT model considered the seasonal and geographic variability, it is an empirical model whose accuracy is lower than models that use observed surface temperature. And the conclusion that there is no significant difference between one-factor ($T_s$) and multi-factor ($T_s$, $e_s$, $P_s$) regression is inaccurate, because the relation between $T_m$ and $T_s$, $e_s$, $P_s$ is more than a simple linear relation.

In this study, we first studied the relationship between $T_m$ and $T_s$, $e_s$, $P_s$ respectively and determined the $T_m-T_s, e_s$ relationship. To make the relationship optimum, we then made seasonal and geographic corrections to the $T_m-T_s, e_s$ and $T_m-T_s$ relationships. To validate the accuracy of the new models, several datasets were employed to examine the models in comparison with the Bevis $T_m-T_s$ relationship at last.

## 2 Data sets

At present, free access to radiosonde data of over 1,000 radiosonde stations for many years is available on the Integrated Global Radiosonde Archive (IGRA) (Durre et al. 2006) website (http://www.ncdc.noaa.gov/oa/climate/igra). Approximate 700 of the total stations have observation data in 80 % of the whole year (Yu 2011). All the radiosonde data used in this paper are from the IGRA. Data found in the IGRA come from radiosondes usually launched twice daily at each station with an interval of 12 h and record the observations, such as pressure, geopotential height, temperature, dew point temperature and wind speed and direction at different heights of the atmosphere.

In addition to the radiosonde data, meteorological data provided by COSMIC can also be used to calculate $T_m$. The COSMIC program (Ding 2009), which was supported by the agencies from the USA and Taiwan area at the end of the last century, is aiming at conducting space science experiments for monitoring the atmosphere. The COSMIC meteorological data, including temperature, vapor pressure, atmospheric pressure and refractive index at different heights of the atmosphere, can be used to calculate $T_m$ by integration. What must be pointed out is that the COSMIC data are not true independent observations, because auxiliary information from European Centre for Medium-Range Weather Forecasts (ECMWF)'s Numerical Weather Prediction (NWP) data are employed to help derive temperature, vapor pressure and pressure from the COSMIC data. Theoretically, the COSMIC system can provide daily 3,000 profiles of the atmospheric elements worldwide with a relatively high vertical resolution of about 0.5 km and a horizontal resolution of about 300 km.

"GGOS (Beutler and Rummel 2012) Atmosphere" is a project carried out at the Vienna University of Technology that is aiming at establishing models of the atmosphere and its website provides $T_m$ globally on $2^\circ \times 2.5^\circ$(lat $\times$ lon) grids every 6 h (http://ggosatm.hg.tuwien.ac.at/). "GGOS Atmosphere" $T_m$ values are calculated from operational analysis data of the ECMWF with a 6-h time resolution by an integral equation.

## 3 The relationship between weighted mean temperature and surface temperature, surface water vapor pressure

In most cases, we cannot know exactly the vertical profiles of the water vapor pressure and temperature, but can get water vapor pressure and temperature observations at specific heights which can be used to calculate weighted mean temperature by numerical integration. The formula is as follows:

$$T_m = \frac{\sum \frac{e_i}{T_i} \cdot \Delta h_i}{\sum \frac{e_i}{T_i^2} \cdot \Delta h_i} \tag{8}$$

where $e_i$ and $T_i$ are the mean water vapor pressure (hPa) and mean temperature (Kelvin) of the atmosphere at the $i$th layer respectively and $\Delta h_i$ is the atmosphere thickness (meter) of the $i$th layer. Only when the layered water vapor pressure and temperature observations are available, we can use this method to calculate $T_m$. And for a given observational accuracy, the higher the vertical resolution of the observations, the more accurately the $T_m$ is calculated. This method is suitable for $T_m$ calculation with radiosonde data or COSMIC data. Though everyone can access accurate $T_m$ from "GGOS Atmosphere", "GGOS Atmosphere" has a 1-day delay to pro-

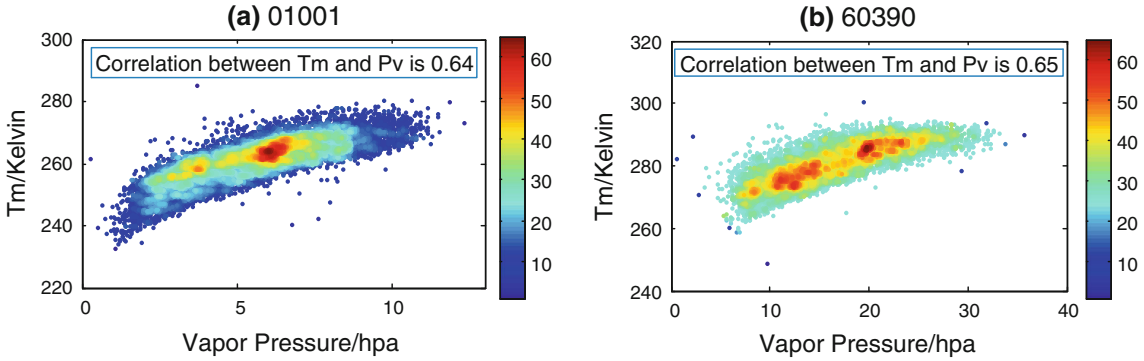


**Fig. 1** Plots of $T_m$ versus $e_s$ from 1995 to 2011 at radiosonde stations 01001 and 60390 (*color* indicates data density)

vide $T_m$ using measured data (it can provide $T_m$ in real time if using forecasting data), so finding a simpler but accurate way to calculate $T_m$ is of practical value for applications of real-time ground-based GPS meteorology. Like Bevis et al. (1992) calculated $T_m$ from surface temperature, we will consider the impact of multi-parameters including surface temperature, water vapor pressure and pressure. In this part, we will investigate the relation between $T_m$ and multi-meteorological parameters and determine the multi-factor $T_m$ model.

### 3.1 Weighted mean temperature versus surface water vapor pressure

Figure 1 shows the plots of $T_m$ (obtained by computation from IGRA data) versus $e_s$(from IGRA) from 1995 to 2011 at radiosonde stations 01001 (01001 is the station ID, N70.93° W8.67°) and 60390 (N36.72° E3.25°). In Fig. 1, for a particular $e_s$, the range of corresponding $T_m$ is not wide (<20 K). The linear regression analysis shows that the correlation coefficients between $T_m$ and $e_s$ are 0.64 at station 01001 and 0.65 at station 60390, while the RMSE of the linear regression is 4.05 and 3.67 K respectively, indicating that there is some correlation between $T_m$ and $e_s$.

In order to determine the optimal relation between $T_m$ and $e_s$, we tried to use some mathematical equations to fit the relation. After experiments with MATLAB cftools, we finally found that the power equation could better fit the relation than the other equations (e.g., the linear polynomial, the quadratic polynomial, the logarithmic equation, etc.). The experimental results of the fitting method are shown in Fig. 2 and Table 1.

The power curve in Fig. 2 achieves good fitting, well expressing the varying trend of $T_m$ with $e_s$ in the whole intervals. Table 1 contains the fitting equation of the power method and information about the fitting precision.

The results in Table 1 show that the power equation could fit well $T_m$ versus $e_s$ with RMS of 3.74 K, indicating that the relation between $T_m$ and $e_s$ could be determined as:

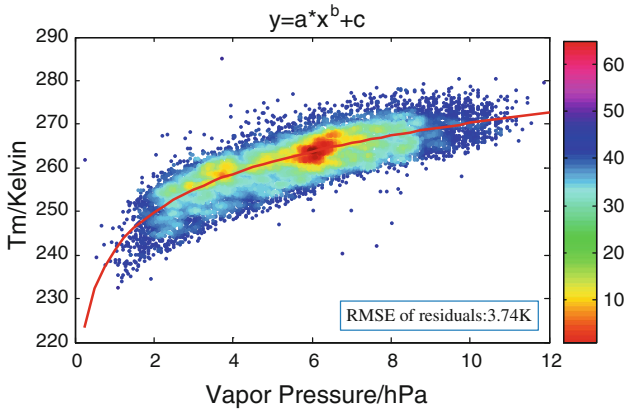


**Fig. 2** Plots of the $T_m$ versus $e_s$ and fitting curves of four fitting equations (*color* indicates data density)

**Table 1** Fitting equations of the power model and information about fitting precision

| Fitting equations | Coefficients | | | RMS (K) |
|---|---|---|---|---|
| | *a* | b | c | |
| $y = a + bx^c$ | −5,174 | 5,415 | 0.002341 | 3.74 |

$$T_m = a + be_s^c \tag{9}$$

### 3.2 The $T_m - T_s$, $e_s$ relationship

After investigating the relation between $T_m$ and $P_s$, we found no correlation between them. As the linear relation between $T_m$ and $T_s$ has been well known, together with the power relation between $T_m$ and $e_s$, we determined the relation between $T_m$ and $T_s$, $e_s$ as follows:

$$T_m = a + bT_s + ce_s^d \tag{10}$$

Radiosonde data ($T_s$, $e_s$ and derived $T_m$ data) from 2001 to 2010 at 135 stations (in Fig. 3) around the globe are used to calculate the coefficients of Eq. (10) as well as the linear regression equation. Excluding the erroneous data and data

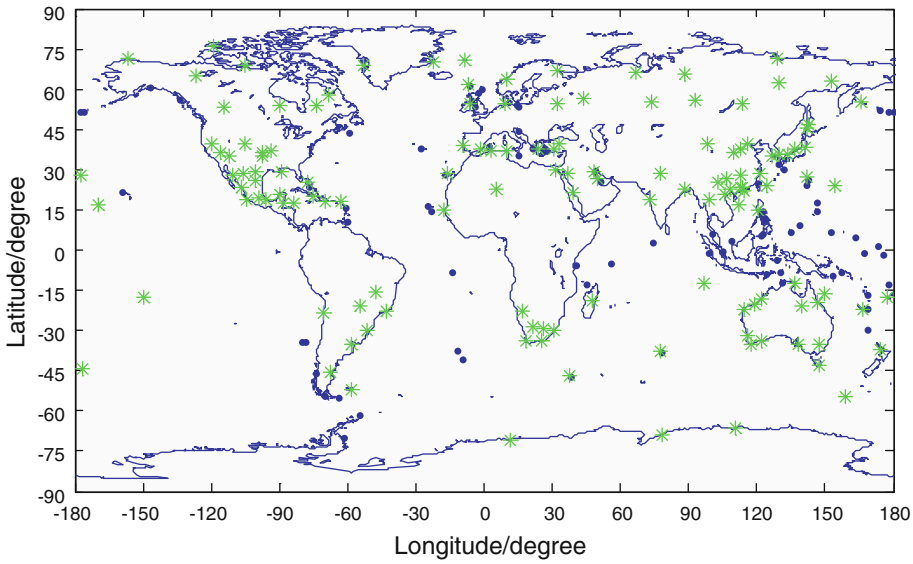


**Fig. 3** Global distribution of 135 radiosonde stations involved in the fitting model

**Table 2** Statistics of mean bias and RMSE between $T_m$ from four models and $T_m$ from radiosonde data at 433 stations unit: Kelvin

| Models | Bias | | | RMSE | | |
|---|---|---|---|---|---|---|
| | Mean | Min | Max | Mean | Min | Max |
| BTm | −0.94 | −12.72 | 5.34 | 4.46 | 1.60 | 13.70 |
| GTm | −0.90 | −10.19 | 5.55 | 4.40 | 1.56 | 11.47 |
| PTm | −0.82 | −9.13 | 4.48 | 3.93 | 1.82 | 10.31 |

with less than 20 layers or observation heights lower than 12 km, there are 256,381 radiosonde observations involved in the fitting model.

The fitted equations are as follows:

$$T_m = 43.69 + 0.8116T_s \quad (11)$$

$$T_m = 81.90 + 0.5344T_s + 31.81e_s^{0.1131} \quad (12)$$

where the units of $T_s$ and $e_s$ are Kelvin and hPa. The RMSE of Eqs. (11), (12) between model values and true values are 4.23, 3.71 K; the multi-factor ($T_s$ and $e_s$) model is about 0.5 K better than the one-factor ($T_s$) model. In order to assess the accuracy of two equations in computing $T_m$, $T_s$, $e_s$ and $T_m$ data from 2001 to 2010 at 433 radiosonde stations around the globe are used to examine the two equations, in comparison with the Bevis $T_m - T_s$ relationship as well. The test results are shown in Table 2. For simplicity's sake, the Bevis $T_m - T_s$ relationship is called the BTm model, Eq. (11) is called the GTm model, and Eq. (12) is called the PTm model.

Statistics in Table 2 shows that the multi-factor model PTm is better than the one-factor model (BTm and GTm) in terms of mean bias and RMSE. The RMSE of the multi-factor model is reduced by $\sim 0.5$ K relative to the one-factor models, in line with previous results. Though the multi-factor model could improve the performance of the one-factor model to some degree, the effect is not significant.

## 4 Seasonal corrections for $T_m$

Yao et al. (2012) studied the residuals of the Bevis $T_m - T_s$ relationship and found that there was a high correlation between the residuals and time. Therefore, to improve a $T_m$ model, not only the impact of multi-meteorological elements should be considered, but also the seasonal variations of $T_m - T_s$, $e_s$ relationship.

In order to research on the residuals of one-factor model (GTm) and multi-factor model (PTm), we treat the "GGOS Atmosphere" $T_m$ data as true values and compute the difference (true values − model values) between true values and model values. Figure 4 shows the residual sequences of the GTm model and the PTm model from 2005 to 2011 at three locations, in which the Fig. 4a, b represents residuals at N0°E7.5°, Fig. 4c, d at N20°E180° and Fig. 4e, f at N60°E160°.

Figure 4 shows the residuals of the GTm model and the PTm model at three different locations, which have been fitted by nonlinear periodic functions (green curves in Fig. 4). These functions are trigonometric functions that consist of an annual cycle and a semi-annual cycle, and they express well the changes of $T_m$ over time. Examined by large amounts of data, the residuals of the GTm model and the PTm model show a high correlation with time and mainly annual variations, but in some regions also accompanied by semi-annual variations. The amplitude of the residuals is larger at high latitudes, smaller at low latitudes, indicating that the relation between $T_m$ and meteorological parameters varies with time as well as locations, and ignoring these will inevitably cause uncertainties.

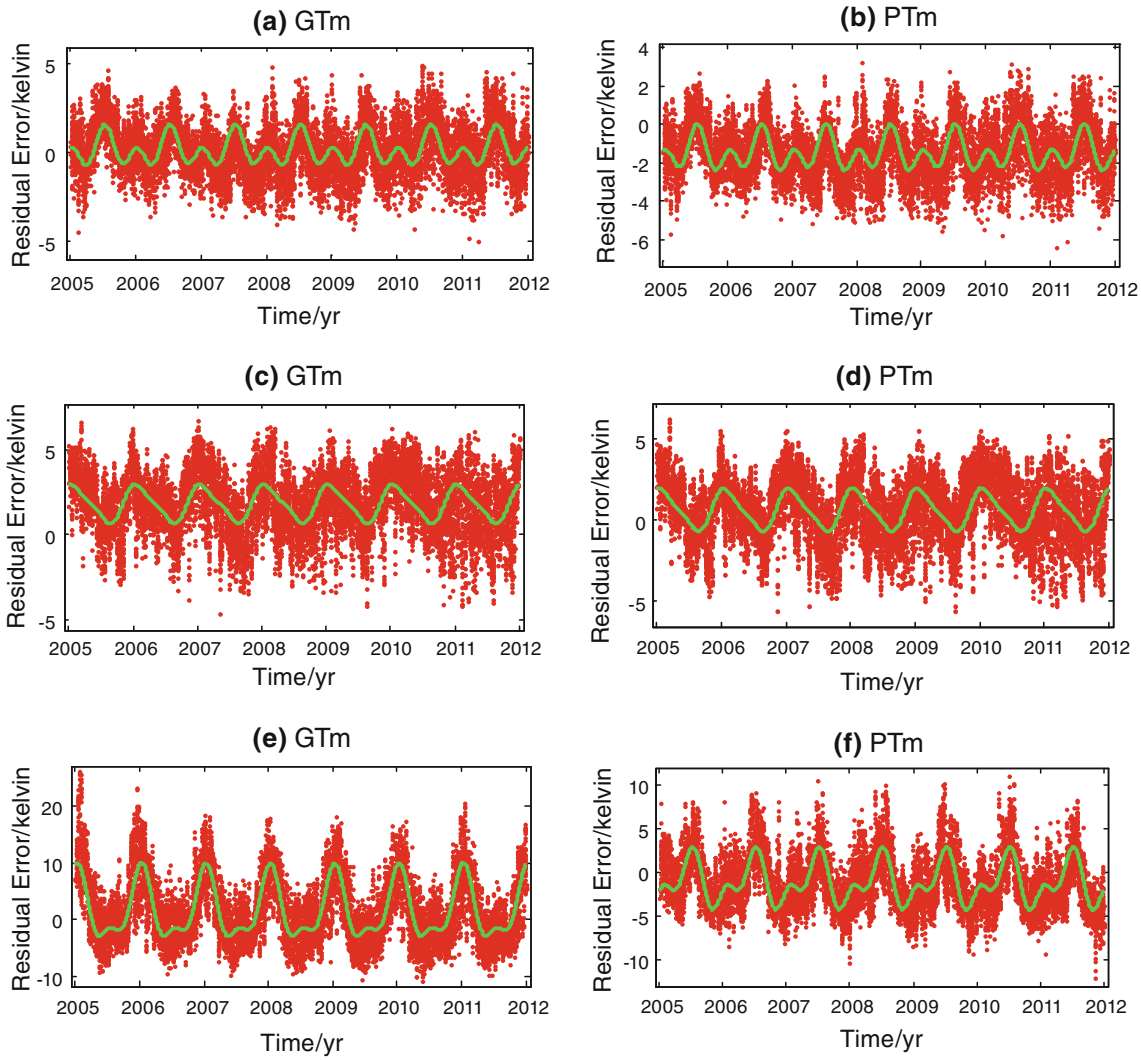


**Fig. 4** Residuals (true values − model values) of the GTm model and the PTm model from 2005 to 2011 at N0°E7.5°, N20°E180° and N60°E160° with respect to GGOS atmosphere data

Böhm et al. (2007) used the trigonometry functions with an annual cycle to reflect the seasonal variations of temperature and pressure in the Global Pressure and Temperature (GPT) model. Lagler et al. (2013) improved the GPT model by estimating amplitudes and phases of the annual and semi-annual amplitudes, yielding the GPT2 model. Learning from the improvement of the GPT2 model, we employ the trigonometry functions with an annual and a semi-annual cycle to model the residuals of the GTm model or the PTm model. Values from the trigonometry functions are treated as seasonal corrections which would then be added to model values from the GTm or PTm model. By this way, we avoid computing model coefficients for different seasons and make the new model more complete and conform to practical situations. If the value of weighted mean temperature from the GTm (PTm) model is $T_{m0}$, and corresponding seasonal correction is $\Delta T_m$, the final weighted mean temperature can be expressed as:

$$T_m = T_{m0} + \Delta T_m \tag{13}$$

$$\Delta T_m = \alpha_0 + \alpha_1 \cos(2\pi^* \text{doy}/365.25) + \alpha_2 \sin(2\pi^* \text{doy}/365.25) + \alpha_3 \cos(4\pi^* \text{doy}/365.25) + \alpha_4 \sin(4\pi^* \text{doy}/365.25) \tag{14}$$

where doy is day of year, $\alpha_0$, $\alpha_1$, $\alpha_2$, $\alpha_3$ and $\alpha_4$ are coefficients of the seasonal correction function. Now that the basics are in place, Eqs. (11)–(14) form the basic frameworks of our new $T_m$ model. It should be noted that the coefficients of Eq. (14) should be computed according to geographic locations, only in this way could the new model achieve the best results.

2° × 2.5°(lat × lon) "2 meter temperature" and "2 meter dew point temperature" (used to compute water vapor pressure) from ECMWF Interim Reanalysis (Dee et al. 2011) from 2005 to 2011 are used to calculate $T_m$ according to Eq. (11) or Eq. (12). Then we calculate the difference (true values−model values) between computed values

and "GGOS Atmosphere" $T_m$, and obtain the $T_m$ residual sequences of 7 years at 13,104 grid points. Utilizing the residual sequences and corresponding day of year, we could convert Eq. (14) to linear equations which are then solved by a least square method. When the coefficients $\alpha_0$, $\alpha_1$, $\alpha_2$, $\alpha_3$ and $\alpha_4$ at 13,104 grid points are computed respectively, the new model is ultimately established. If $T_{m0}$ is derived from the GTm model or the PTm model, the new model is called GTm-I or PTm-I, correspondingly (Matlab code and tables of coefficients for GTm-I and PTm-I are provided as electronic supplements). When we want to calculate $T_m$ at some site, we first use Eq. (11) or (12) to calculate $T_{m0}$ according to the meteorological parameters; then according to the latitude and longitude of the site, we use Eq. (14) to calculate seasonal corrections at four grid points that are nearest to the site; afterwards, the bilinear interpolation is employed to calculate the seasonal correction $\Delta T_m$ at the site; finally, we obtain $T_m$ by adding up $T_{m0}$ and $\Delta T_m$.

## 5 Validation of the new models

In Sects. 3 and 4, we established the one/multi-parameter $T_m$ model GTm-I and PTm-I which took the seasonal and geographic variations into consideration. In this section, the new models will be tested and compared to verify their performance.

The GTm-I and PTm-I models are first examined by the global radiosonde data in the whole 2010 at 277 stations in comparison with the Bevis $T_m - T_s$ relationship (for simplicity, we call it BTm). Table 3 shows the statistics of the test results.

According to the statistics in Table 3, the GTm-I and the PTm-I improved the accuracy of $T_m$ estimation by 13.2 %, 21.1 % respectively relative to the BTm model, and the multi-factor model PTm-I has a better accuracy than the one-factor model GTm-I. From the comparison between Tables 2 and 3, we can see that the GTm-I model and the PTm-I model further improve the accuracy of the GTm model and the PTm model, which should be owed to that the new model considered the seasonal and geographic variations. Overall, the PTm-I model is better than the other models.

We compared the $T_m$ from radiosonde data and those from "GGOS Atmosphere" and those from the COSMIC, finding that the "GGOS Atmosphere" $T_m$ data have a bias of 0.16 K and RMSE of 2.2 K and the COSMIC-derived $T_m$ data have a bias of -0.06 K and RMSE of 1.94 K relative to the $T_m$ data from radiosonde observations. So these $T_m$ data from different sources have some differences.

As the coefficients of Eq. (14) were computed based on the "GGOS Atmosphere" $T_m$ grid data, so the GTm-I model and the PTm-I model, which have been corrected by Eq. (14), ought to better conform to the "GGOS Atmosphere" $T_m$ data than the radiosonde data. So only the "GGOS Atmosphere" $T_m$ data could exclude the data differences and actually examine the correctness and performance of the GTm-I model and the PTm-I model. We use the "GGOS Atmosphere" $T_m$ data in whole 2012 to examine the two models, and the test results are shown in Table 4.

Statistics in Table 4 shows that the global mean bias of the GTm-I model and the PTm-I model is all around 0.1 K, this indicates that taking the seasonal and geographic variations into consideration could effectively reduce systematic biases. The GTm-I model and the PTm-I model both have small RMSE ($< 3$ K), and improved the accuracy by 33.2 and 35.8 % respectively relative to the BTm model. Comparisons between the two new models show that the multi-factor model (PTm-I) is no longer superior to the one-factor model (GTm-I), this is because the residuals of the GTm model contained the errors caused by one-factor model and these errors have been corrected by Eq. (14) to some degree. Tested by comparing with the "GGOS Atmosphere" data, the two models obtained objective test results that could reflect the performance of the models and the correctness of the modeling method. Figure 5 shows the global distribution of the accuracy of the three models.

The global distribution of the accuracy of the four models has been shown in Fig. 5, according to which we could intuitively know where the models have a high accuracy and where the accuracy becomes low, this is very important to the users. Comparing Fig. 5a, c and e, we could find that the BTm model has large systematic biases ($>5$ K) around the eastern coast of the Pacific, in Greenland, in the Antarctic areas and in the Himalayan regions, while the other two models both have small biases, which further indicates that it is necessary to consider the seasonal and geographic variations when establishing $T_m$ models. Comparing Fig. 5b, d and f,

**Table 3** Mean bias and RMSE between models (BTm, GTm-I, PTm-I) and sounding data in whole 2010 at 277 stations

| Models | Bias (K) | | | RMSE (K) | | |
|---|---|---|---|---|---|---|
| | Mean | Min | Max | Mean | Min | Max |
| BTm | −0.42 | −13.05 | 5.52 | 4.40 | 0.79 | 14.14 |
| GTm-I | −0.47 | −9.51 | 8.86 | 3.82 | 1.06 | 11.24 |
| PTm-I | −0.59 | −9.84 | 8.31 | 3.47 | 1.01 | 10.77 |

**Table 4** Mean bias and RMSE of the BTm model, the GTm-I model and the PTm-I model tested by comparing with respect to the "GGOS Atmosphere" $T_m$ data in 2012

| Models | Bias (K) | | | RMSE (K) | | |
|---|---|---|---|---|---|---|
| | Mean | Min | Max | Mean | Min | Max |
| BTm | −0.88 | −14.56 | 7.38 | 3.86 | 1.12 | 15.13 |
| GTm-I | −0.11 | −10.00 | 1.61 | 2.58 | 0.95 | 10.67 |
| PTm-I | −0.10 | −10.03 | 1.77 | 2.48 | 0.97 | 10.46 |

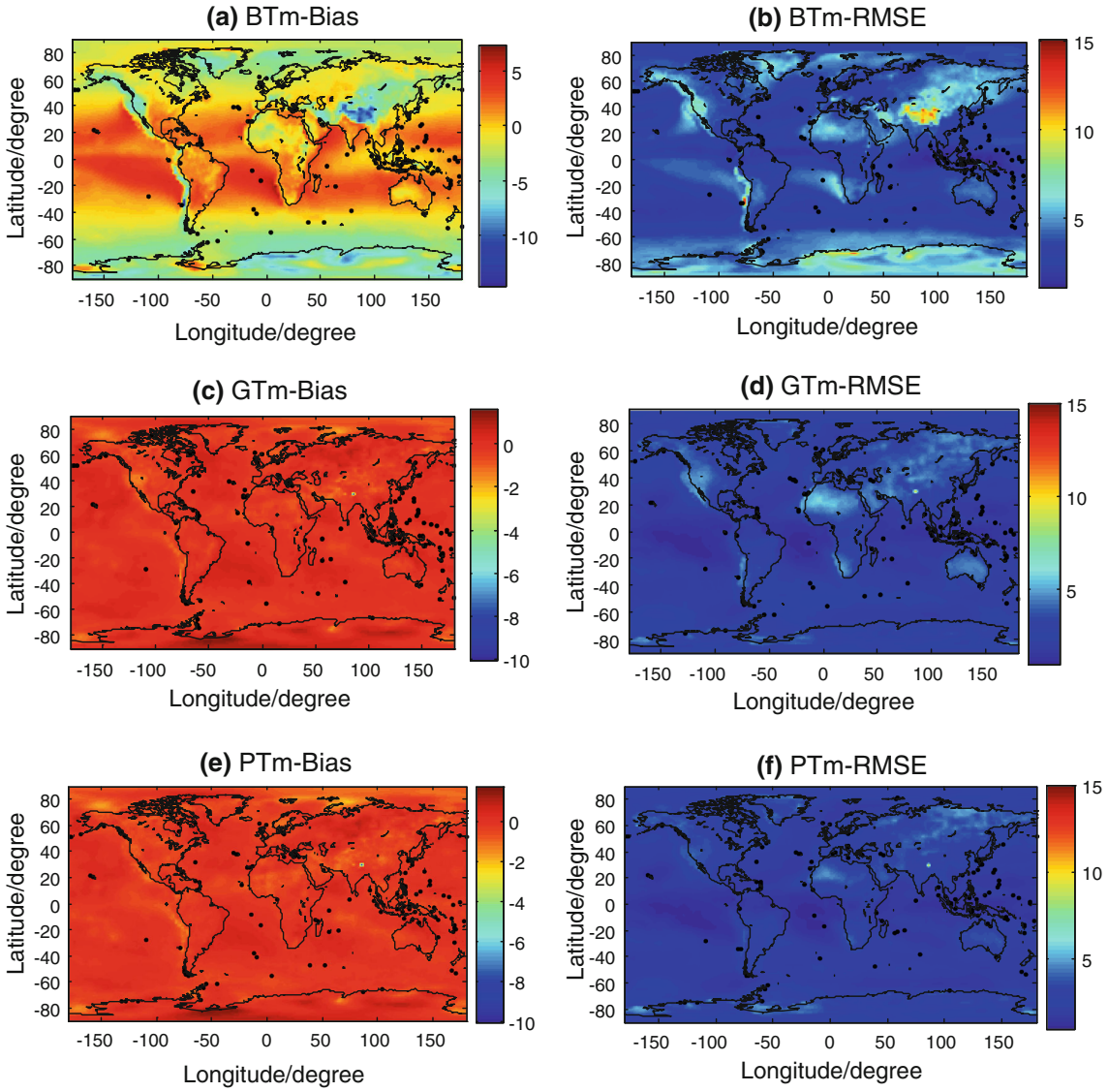


**Fig. 5** Global distribution of mean bias and mean RMSE between "GGOS Atmosphere" data and the four models in 2012

we could see that the BTm model has large errors around the eastern coast of the Pacific, in Greenland, in the Antarctic areas and in the Himalayan regions too, and these errors got reduced by the GTm-I model on a global scale, and further reduced by the PTm-I model in the Asian areas and African areas. In addition to these, the GTm-I model and the PTm-I model both achieve an approximately consistent high accuracy, proving the effectiveness of the modeling method in this paper.

The COSMIC-derived $T_m$ data in 2010 are also employed to further examine the GTm-I model and the PTm-I model in comparison with the BTm model. We calculated the daily bias and RMSE of the models in the early 346 days of 2010 (as only these data are available), and the overall statistics of the test results is shown in Table 5, daily RMSE is shown in Fig. 6.

**Table 5** Mean bias and RMSE between the four models and COSMIC-derived $T_m$ data in early 346 days of 2010

| Models | Bias (K) | | | RMSE (K) | | |
|---|---|---|---|---|---|---|
| | Mean | Min | Max | Mean | Min | Max |
| BTm | −0.42 | −1.26 | 0.54 | 3.90 | 3.51 | 4.31 |
| GTm-I | 0.16 | −0.35 | 0.61 | 2.94 | 2.52 | 3.39 |
| PTm-I | 0.80 | 0.18 | 1.34 | 3.20 | 2.60 | 4.30 |

Figure 6 shows that the RMSE of the BTm model is larger than that of the GTm-I model and the PTm-I model almost every day in the early 346 days of 2010, while the GTm-I model is very stable, and achieves a high accuracy. The accuracy of the PTm-I model is a little lower than the GTm-I model and larger fluctuations appear, but it is still superior to

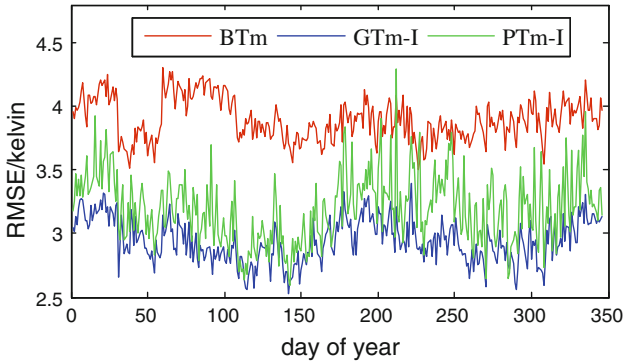


**Fig. 6** Daily RMSE of the three models in the early 346 days of 2010 compared with COSMIC-derived $T_m$ data

**Table 6** Statistics of mean RMSE and maximum RMSE between the new models and the BTm model

| ΔPWV | Mean RMSE (mm) | Max RMSE (mm) |
|---|---|---|
| $PWV_1 - P_0$ | 0.2 | 0.6 |
| $PWV_2 - PWV_0$ | 0.3 | 2.1 |

the BTm model. Table 5 together with Fig. 6 both show that the GTm-I model performs the best, then the PTm-I model, and the last is still the BTm model.

At last, ZWD data from "GGOS Atmosphere" and surface temperature data and vapor pressure data from ECMWF are used to validate the improvement with the new models for $T_m$ in terms of precipitable water. We calculate $T_m$ with the BTm model, the GTm-I model and the PTm-I model respectively, then map ZWD to PWV according to Eqs. (1)–(2). By this method, we computed the PWV at the global $2° \times 2.5°$ grid points. PWV with BTm model is marked as PWV0, PWV with GTm-I model is marked as PWV1, and PWV with PTm-I is marked as PWV2. RMSE of residuals of $\mathrm{PWV}_i - \mathrm{PWV}_0 (i = 1, 2)$ is computed at every grid point. Statistics of mean RMSE and maximum RMSE is shown in Table 6.

In Table 6, the global mean RMSE of $\Delta PWV$ is 0.2–0.3 mm between PWV with the new $T_m$ models and the BTm model. This RMSE is small in average because the global mean PWV is small ($\sim$ 18.4 mm in 2012). However, in the tropics where the PWV is large (the maximum is 82.8 in 2012), the RMSE can become as large as more than 2 mm.

## 6 Conclusions

This paper studied the relation between weighted mean temperature and surface temperature, surface water vapor pressure, surface pressure, and found that weighted mean temperature is highly correlated with surface temperature and surface water vapor pressure, but unrelated to surface pressure. Based on these, we determined the non-linear relation (Eq. 12) between weighted mean temperature and surface temperature, surface water vapor pressure. Examined by comparing with the radiosonde data, the weighted mean temperature–surface temperature and surface water vapor pressure relationship (Eq. 12) improved the accuracy by 0.5 K relative to the weighted mean temperature–surface temperature relationship.

Considering the seasonal and geographic variations in the weighted mean temperature–surface temperature and surface water vapor pressure or weighted mean temperature–surface temperature relationship, we should make corresponding corrections. Periodical variations were observed in the residuals of the GTm model and the PTm model when we were analyzing the residuals. Based on this, we employed the trigonometry functions with an annual and a semi-annual cycle to fit the residuals of the two models. The fitted functions are used to correct the original models (GTm, PTm), and by this way the accuracy of the original models is improved. Taking the geographic variations into account, we computed the coefficients of Eq. (14) at $2° \times 2.5°$ grid points, and finally established the GTm-I and PTm-I model. Examined by radiosonde data, "GGOS Atmosphere" data and COSMIC data, the GTm-I and PTm-I model both achieved a 1.0 K higher accuracy (see Tables 3, 4, 5) than the widely used BTm model. It has to be noted that the multi-factor model is no longer superior to the one-factor model after seasonal corrections are made.

**Acknowledgments** The authors would like to thank IGRA for providing access to the web-based IGRA data and "GGOS Atmosphere" for providing grids of $T_m$ and COSMIC for the occultation data and ECMWF for temperature and dew point temperature data. We will also thank Prof. Johannes Böhm for his kind help. This research was supported by the National Natural Science Foundation of China (41174012; 41274022) and The National High Technology Research and Development Program of China (2013AA122502).

## References

Askne J, Nordius H (1987) Estimation of tropospheric delay for microwaves from surface weather data. Radio Sci 22(3):379–386

Bevis M, Businger S, Herring TA, Rocken C, Anthes RA, Ware RH (1992) GPS meteorology: remote sensing of atmospheric water vapor using the global positioning system. J Geophys Res 97(D14):15,787–15,801

Bevis M, Businger S, Chiswell S, Herring TA, Anthes RA, Rocken C, Ware RH (1994) GPS meteorology: mapping zenith wet delays onto precipitable water. J Appl Meteor 33(3):379–386

Bevis M, Businger S, Chiswell S, (1995) Earth-based GPS meteorology: an overview. American Geophysical Union 1995 fall meeting, EOS, Transactions, vol 76, issue no 46. American Geophysical Union

Beutler G, Rummel R (2012) Scientific rationale and development of the global geodetic observing system. In: Geodesy for planet earth. Springer, Berlin, pp 987–993

Böhm J, Heinkelmann R, Schuh H (2007) Short Note: a global model of pressure and temperature for geodetic applications. J Geod 81(10):679–683

Davis JL, Herring TA, Shapiro II, Rogers AEE, Elgered G (1985) Geodesy by radio interferometry: effects of atmospheric modeling errors on estimates of baseline length. Radio Sci 20:1593–1607

Dee DP, Uppala SM, Simmons AJ, Berrisford P, Poli P, Kobayashi S, Vitart F et al (2011) The ERA-interim reanalysis: configuration and performance of the data assimilation system. Q J R Meteorol Soc 137(656):553–597

Ding JC (2009) GPS meteorology and its applications. China Meteorological Press, Beijing, pp 1–10

Durre I, Vose RS, Wuertz DB (2006) Overview of the integrated global radiosonde archive. J Climate 19(1):53–68

Jacob D (2001) The role of water vapour in the atmosphere. A short overview from a climate modeller's point of view. Phys Chem Earth (A) 26(68):523–527

Lagler K, Schindelegger M, Böhm J, Krásná H, Nilsson T (2013) GPT2: empirical slant delay model for radio space geodetic techniques. Geophys Res Lett. doi:10.1002/grl.50288

Li JG, Mao JT, Li CC (1999) The approach to remote sensing of water vapor based on GPS and linear regression $T_m$ in eastern region of China. Acta Meteor Sin 57(3):283–292

Rocken C, Ware R, VanHoveT Solheim F, Alber C, Johnson J, Bevis M, Businger S (1993) Sensing atmospheric water vapor with the global positioning system. Geophys Res Lett 20(23):2631–2634. doi:10.1029/93GL02935

Ross RJ, Rosenfeld S (1997) Estimating mean weighted temperature of the atmosphere for global positioning system applications. J Geophys Res 102(D18):21,719–21,730

Wang XY, Song LC, Dai ZQ, Cao YC (2011) Feature analysis of weighted mean temperature $T_m$ in Hong Kong. J Nanjing Univ Inf Sci Technol Nat Sci Edn 3(1):47–52

Wang Y, Liu LT, Hao XG, Xiao JH, Wang HZ, Xu HZ (2007) The application study of the GPS meteorology network in Wuhan region. Acta Geodaetica et Cartographica Sinica 36(2):142–145

Yao YB, Zhu S, Yue SQ (2012) A globally applicable, season-specific model for estimating the weighted mean temperature of the atmosphere. J Geod 86(12):1,125–1,135

Yu SJ (2011) Remote sensing of water vapor based on ground GPS observations. Ph.D. dissertation, Institute of Geodesy and Geophysics, Chinese Academy of Sciences, Wuhan